nature communications

Article

https://doi.org/10.1038/s41467-024-52005-1

Pro-efferocytic nanotherapies reduce vascular inflammation without inducing anemia in a large animal model of atherosclerosis

Received: 27 August 2023

Accepted: 22 August 2024

Published online: 13 September 2024

Check for updates

Sharika Bamezai[1,10], Yapei Zhang[2,3,10], Manisha Kumari[2,3,10], Mozhgan Lotfi[1], Tom Alsaigh[1], Lingfeng Luo[1], Gayatri Suresh Kumar[1], Fudi Wang[1], Jianqin Ye[1], Madhu Puri[2,3], Romila Manchanda[2,3], Sesha Paluri[2,3], Shaunak S. Adkar[1], Yoko Kojima[1], Alice Ingelsson[1], Caitlin F. Bell[1], Nicolas G. Lopez[1], Changhao Fu[1], Ryan B. Choi[1], Zach Miller[2], Leo Barrios[2], Susan Walsh[4], Ferhaan Ahmad[4], Lars Maegdefessel[5,6,7], Bryan Ronain Smith[2,3,11] ✉ & Nicholas J. Leeper[1,8,9,11] ✉

Atherosclerosis is an inflammatory disorder responsible for cardiovascular disease. Reactivation of efferocytosis, the phagocytic removal of cells by macrophages, has emerged as a translational target for atherosclerosis. Systemic blockade of the key 'don't-eat-me' molecule, CD47, triggers the engulfment of apoptotic vascular tissue and potently reduces plaque burden. However, it also induces red blood cell clearance, leading to anemia. To overcome this, we previously developed a macrophage-specific nanotherapy loaded with a chemical inhibitor that promotes efferocytosis. Because it was found to be safe and effective in murine studies, we aimed to advance our nanoparticle into a porcine model of atherosclerosis. Here, we demonstrate that production can be scaled without impairing nanoparticle function. At an early stage of disease, we find our nanotherapy reduces apoptotic cell accumulation and inflammation in the atherosclerotic lesion. Notably, this therapy does not induce anemia, highlighting the translational potential of targeted macrophage checkpoint inhibitors.

Atherosclerotic cardiovascular disease is a leading cause of death in the United States[1]. Although risk-reducing therapies directed against hypertension, dyslipidemia, and smoking have improved clinical outcomes, these approaches have failed to ameliorate the public health impact of myocardial disease and stroke[2]. Accordingly, there is a need to develop novel treatments that target the mechanisms underlying atherogenesis, such as chronic inflammation. However, targeting fundamental inflammatory pathways such as IL1β can result in

[1]Department of Surgery, Division of Vascular Surgery, Stanford University School of Medicine, Stanford, CA, USA. [2]Department of Biomedical Engineering, Michigan State University, East Lansing, MI, USA. [3]Institute for Quantitative Health Science and Engineering, East Lansing, MI, USA. [4]Division of Cardiovascular Medicine, Department of Internal Medicine, University of Iowa Carver College of Medicine, Iowa City, IA, USA. [5]Department for Vascular and Endovascular Surgery, Klinikum rechts der Isar, Technical University, Munich, Germany. [6]German Center for Cardiovascular Research, partner site Munich Heart Alliance, Berlin, Germany. [7]Department of Medicine, Karolinska Institutet, Stockholm, Sweden. [8]Department of Medicine, Division of Cardiovascular Medicine, Stanford University School of Medicine, Stanford, CA, USA. [9]Stanford Cardiovascular Institute, Stanford, CA, USA. [10]These authors contributed equally: Sharika Bamezai, Yapei Zhang, Manisha Kumari. [11]These authors jointly supervised this work: Bryan Ronain Smith, Nicholas J. Leeper. ✉e-mail: smit2901@msu.edu; nleeper@stanford.edu

immunosuppression, as evidenced by increased rates of fatal infection in patients receiving Canakinumab in the CANTOS trial[3]. These results highlight the need for additional (immuno)therapeutic approaches with orthogonal mechanisms of action and more favorable side effect profiles.

Among the many emerging translational targets in the field of cardiovascular medicine, a phenomenon known as efferocytosis has recently been prioritized for study[4]. Efferocytosis refers to the engulfment and clearance of pathological cells by professional phagocytes such as macrophages[5]. Within the atherosclerotic plaque, enlargement of the necrotic core is, in part, a consequence of impaired removal of apoptotic vascular cells, which have upregulated the key anti-phagocytic 'don't-eat-me' molecule CD47 on their surface[6]. The growth of a necrotic core contributes to plaque instability and eventual rupture, which serves as a nidus for subsequent acute thrombosis[7,8].

Antibodies (Ab) which block the binding of CD47 to its cognate receptor SIRPα potently reduce plaque vulnerability and lesion size by preventing the accumulation of apoptotic debris in murine models of atherosclerosis[6]. These pre-clinical observations were recently extended in a phase I trial of the first humanized anti-CD47 Ab[6,9]. Subjects receiving 'macrophage checkpoint inhibitors' experienced a dramatic reduction in vascular inflammation of the carotid artery, as quantified by serial ^{18}F-fluorodeoxyglucose (FDG)-PET/CT scans[10]. Unfortunately, anti-CD47 Ab treatment in both mouse models and humans has been shown to induce anemia due to the non-specific erythrophagocytosis of aged red blood cells (RBCs) in the spleen[6,9].

Studies demonstrating toxicity of anti-CD47 antibody-mediated blockade therefore prompted a search for methods which could reactivate efferocytosis in a precision-targeted manner. To do this, we generated a macrophage-specific nanotherapy loaded with a chemical inhibitor of Src homology 2 domain-containing phosphatase-1 (SHP-1), a small molecule downstream of the CD47-SIRPα signaling axis[11,12]. This 'Trojan horse' nanoparticle selectively delivered drug to inflammatory monocytes and macrophages (MO/MΦ) within the atherosclerotic plaque, potently augmented phagocytosis, and reduced atherosclerosis as effectively as gold-standard Ab therapies in mouse models[11,12]. Most notably, this therapy did not cause any hematological toxicity[12].

Accordingly, the aim of this study was to test our targeted nanoparticles in a large animal model of cardiovascular disease (CVD) to determine if additional translation of our nanotherapy toward human clinical trials is justified.

Results

'Large batch' SWNTs retain their expected physicochemical properties and induce phagocytosis in vitro

Critical to the success of SWNT-SHP1i nanotherapy is their selectivity to monocytes as a targeted agent. The physicochemical properties of SWNTs dictate their selectivity. We thus tested their size, zeta potential, and chemical properties. The large-batch SWNTs display similar size and surface charge to small-batch SWNTs[11–13]. Dynamic light scattering (DLS) shows the synthesized SWNT and SWNT-Cy5.5-SHP1i have an average 'hydrodynamic diameter' of ~91 nm and ~110 nm, respectively (Fig. 1a). The near-neutral surface charge (1.75 mv) promotes the stability and relatively long half-life of SWNT-Cy5.5-SHP1i in blood circulation (Fig. S1b, c). We confirmed the presence of Cy5.5 fluorescent dye (when Cy5.5 was used) and SHP1i loaded on SWNTs using UV-Vis spectroscopy and Fourier-Transform Infrared spectroscopy (FT-IR). UV-Vis validated the presence of Cy5.5 (sharp peak at ~674 nm) and SHP1i (absorption peaks at ~510 nm and 332 nm) (Fig. 1b and Fig. S1d, which also allowed us to quantify the number of SHP1i molecules per SWNT). The presence of SHP1i on SWNTs was further validated by FT-IR, with the new peak showing at ~2232 cm^{-1} compared with SWNTs (Fig. 1c and Fig. S1e). We studied the release profile of SHP1i from

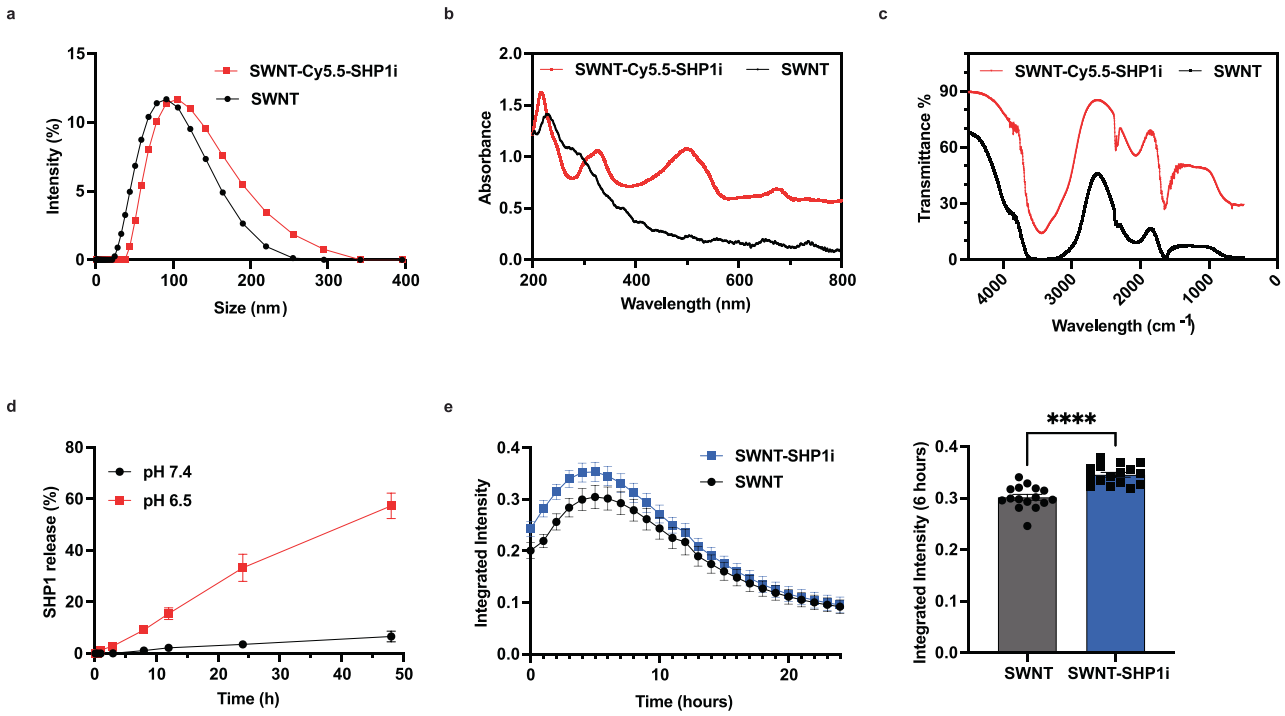


Fig. 1 | 'Large batch' SWNTs retain their expected physicochemical properties and induce phagocytosis in vitro. Physicochemical characterization of large-batch SHP1i-loaded SWNTs displays successful SHP1i loading and release in acidic solutions. **a** DLS; **b** UV-Vis spectroscopy; and **c** FT-IR spectroscopy of SWNT and SWNT-Cy5.5-SHP1i; **d** SHP1i release from SWNTs at neutral and acidic pH. Data are presented as mean values ± SD. $n = 3$ over independent replicates; **e** In vitro Incucyte phagocytosis assay demonstrates large batch SWNT-SHP1i treatment of RAW264.7 macrophages significantly increases phagocytosis of apoptotic cells compared to SWNT treatment. ****$P < 0.0001$ by unpaired two-tailed t-test. Data are presented as mean values ± SEM. $n = 16$ per group over technical replicates. Source data are provided as a Source data file.

SWNTs in PBS at different pH (7.4 and 6.5). We found that SHP1i release is accelerated by more acidic conditions, with pH 6.5 driving more rapid release than pH 7.4 across timepoints (Fig. 1d), as shown with small batch SWNTs[13]. Importantly, less than 6.7% SHP1i was released at pH 7.4, suggesting SWNT-Cy.5.5-SHP1i features longer-term drug retention in blood circulation which displays an approximately neutral pH.

After confirming that the physicochemical properties of 'large-batch' SWNTs were consistent with those generated on a smaller scale for mouse studies, we performed a series of in vitro phagocytosis assays to confirm their functional characteristics. Compared to control SWNT, we found that SWNT-SHP1i increased apoptotic cell engulfment (Fig. 1e and Fig. S1f, $^{****}p < 0.0001$). These increases were consistent with prior publications[12], suggesting that production scaling does not reduce the therapeutic efficacy of our agent, in vitro.

SWNTs are preferentially taken up by monocytes in the circulation

SWNTs are almost exclusively taken up by inflammatory MO/MΦ in mice[12]. To determine if this exquisite selectivity is retained in larger animal models, we performed flow cytometry on blood drawn from pigs 7 days after SWNT injection (Fig. 2a and S2). Using anti-PEG Ab positivity as a surrogate for SWNT uptake (which are otherwise too small and carbon-based to be easily visualized), we found that ~55% of the $CD163^+CD14^-$ monocytes were SWNT positive one week after infusion of either SWNT or SWNT-SHP1i (Fig. 2b). Nearly 5% of $CD163^+CD14^+$ cells showed SWNT uptake in SWNT/SWNT-SHP1i treated pigs and <1% of the $CD163^-CD14^+$ showed SWNT positivity. Very little uptake was observed in any of the other circulating leukocytes studied, including <1% positivity in $CD3^+$ T cells, $CD21^+$ B cells, and $CD8a^+$ NK subset. The $CD163^-CD14^-$, which represents all other immune and non-immune cells exhibited <1% positivity in both groups. No difference was observed in the immune cell composition of the blood at baseline and two weeks after SWNT or SWNT-SHP1i treatment (Fig. S3).

SWNTs preferentially accumulate in the early atherosclerotic lesion and SHP1 inhibition reduces apoptotic cell accumulation in addition to vascular inflammation in vivo

To determine the impact of pro-efferocytic therapies on vascular disease in a large animal model, we randomized 3-month-old $LDLR^{-/-}$ pigs to 12 weekly infusions of SWNT or SWNT-SHP1i (Fig. 3a). Consistent with our blood findings, flow cytometry of the carotid artery showed that MO/MΦ internalized significantly more SWNT/SWNT-SHP1i (45%) than the non-MO/MΦ (7%) cell population (Fig. 3b and Fig. S4, $^{***}p = 0.0001$). Analysis of the iliac artery (60% in MO/MΦ vs 17% in non-MO/MΦ, $^{**}p < 0.01$) and renal artery bifurcation (54% in MO/MΦ vs 16% non-Mo/Mϕ, $^{**}p < 0.01$) confirmed these results in additional vascular beds (Fig. 3b). These findings differed from non-vascular tissue such as the bone marrow, where SWNT/SWNT-SHP1i uptake was low in both the MO/MΦ (16%) and non-MO/MΦ (12%) cell populations (Fig. 3b). Moreover, no significant difference was observed in intralesional uptake by MO/MΦ between the SWNT and SWNT-SHP1i treated groups (Fig. S5).

At this early timepoint in plaque atherogenesis, early fatty streaks were observed in the coronary arteries, and these did not differ in size between conditions (Fig. 3c). However, non-invasive ^{18}F-FDG PET/CT imaging performed prior to sacrifice revealed a significantly lower SUV_{mean} score in the carotid arteries of SWNT-SHP1i treated animals. Left and right carotid artery SUV_{mean} scores were averaged for comparison (Fig. 3d, $^{*}p < 0.05$). This result suggests SWNT-SHP1i nanotherapy may reduce inflammation even before the development of advanced atherosclerotic lesions. Although there was no significant difference in macrophage recruitment in SWNT-SHP1i-treated vessels within the tested timeframe (Fig. 3e), lesions from SWNT-SHP1i treated animals harbored significantly fewer TUNEL-positive apoptotic bodies (Fig. 3f, $^{*}p < 0.05$), suggesting enhanced clearance of cells, which would otherwise accumulate within the developing necrotic core.

Pro-efferocytic therapies induce favorable immunological gene expression changes across species

To understand the biology underlying the physiologic changes reported above, we next performed bulk RNA sequencing of carotid arteries harvested from SWNT- and SWNT-SHP1i-treated pigs (Fig. 4a). A direct comparison of RNA expression between SWNTs and SWNT-SHP1i groups revealed 179 differentially expressed genes (DEGs), of which 152 were upregulated and 27 were downregulated, using a cutoff of >1 log2 fold change and an adjusted p-value of <0.05 (Fig. 4b, Supplementary data 1). Pathway analyses of these differentially regulated genes highlighted alterations in the innate immune response, response to external biotic stimulus, endocytosis, and regulation of cytokine production (Fig. S6).

To identify changes that are likely to be consistent across species, we then integrated RNA sequencing results from the current pig study with single-cell RNA sequencing results from our previously published mouse intervention study[12]. Using this approach, we identified a list of 35 commonly upregulated genes which were consistently activated in response to SWNT-SHP1i therapy (Fig. 4c) Notably, the well-known anti-atherosclerotic gene Heme Oxygenase 1 (HMOX1) was included as a top, highly upregulated gene[14–17]. Pathway analysis of these commonly dysregulated genes confirmed regulation of the immune system, response to an external biotic stimulus, endocytosis, and phagocytosis as themes shared across species after exposure to pro-efferocytic therapy (Fig. 4d).

Pro-efferocytic SWNTs do not induce the hematologic abnormalities associated with anti-CD47 Ab therapy

To confirm the safety of SWNT-SHP1i in our large animal model, we performed a series of toxicity and tolerability studies. In contrast to the anemia and compensatory reticulocytosis observed with non-targeted anti-CD47 Ab therapy[9], we found that SWNT-SHP1i did not induce loss of RBCs or platelets (Fig. 5a). There were also no significant differences in any other CBC lab values including WBCs, neutrophils, lymphocytes, and monocytes at each timepoint (Fig. 5a). SWNT-SHP1i had no deleterious impact on lipid levels, renal function, or hepatic function compared to control SWNT-treated animals (Fig. 5b–d, Fig. S7a). There was no significant difference in body weight between SWNT or SWNT-SHP1i treated pigs at any of the weekly measurements (Fig. 5e). Though some animals did experience mortality midway through the treatment regimen (Fig. S7b), these three deaths were distributed across groups and felt to be secondary to induction of anesthesia, as no deaths were observed after the veterinary team adapted their protocols to use slower anesthetic infusions.

Discussion

This study features several key findings relevant to the translation of targeted nanotherapies from bench-to-bedside through a large animal model. First, we show that SWNT production can be successfully scaled without impairing key SWNT physicochemical properties or predilection for uptake by inflammatory myeloid-lineage cells. Second, we show that these nanoparticles retain their ability to deliver a payload of potent pro-efferocytic therapies to inflamed macrophages and continue to induce anti-inflammatory changes in a large animal model of atherosclerotic cardiovascular disease. Finally, we confirm that this 'precision medicine' approach does not induce the off-target clearance of healthy tissue outside of the vasculature, thus circumventing one of the key limitations observed with the systemic pro-phagocytic antibodies currently in development[6,9]. These results collectively highlight the feasibility of advancing 'Trojan horse' nanoparticles further toward the clinic and underscore the potential of intracellular macrophage checkpoint inhibitors as a promising treatment paradigm for individuals at risk of heart attack and stroke.

https://doi.org/10.1038/s41467-024-52005-1

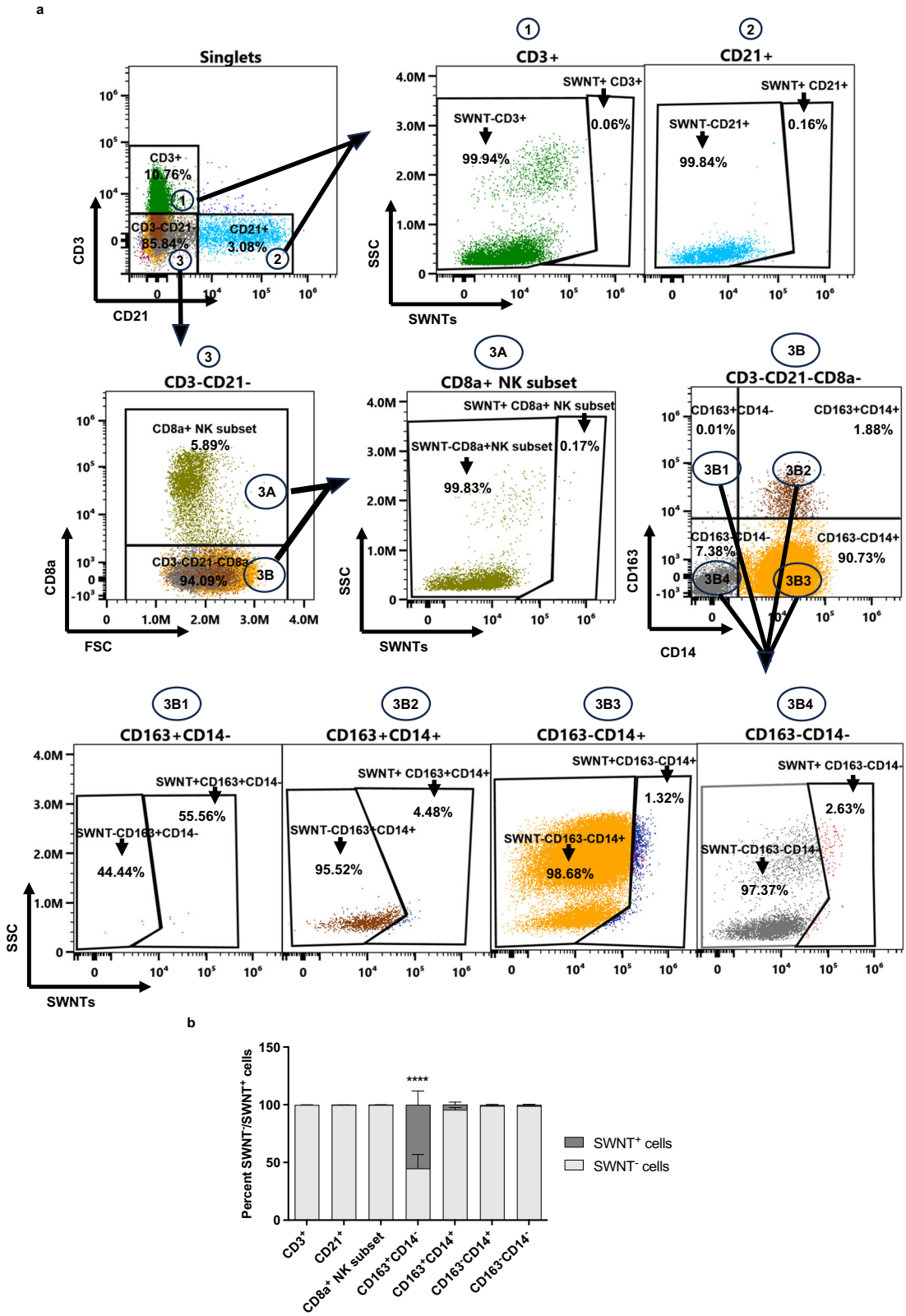


Fig. 2 | SWNTs are preferentially taken up by monocytes in the circulation. SWNTs are preferentially taken up and retained in the circulation by pig blood monocytes and not lymphocytes. **a** Representative dot plots and gating strategy for SWNT uptake and retention by different immune cell types 7 days after injection. $CD3^+$ cells represent T cells, $CD21^+$ cells represent B cells, and $CD8a^+$ cells represent a subtype of Natural killer cells. $CD163^+CD14^-$, $CD163^+CD14^+$, $CD163^-CD14^+$ cells represent different monocyte subtypes, while $CD163^-CD14^-$ represent the remaining immune and non-immune cells. **b** Bar diagram of the percent $SWNT^+$ cells in pig blood 7 days after SWNT or SWNT-SHP1i injection. **** indicates $P < 0.0001$ compared to $CD3^+$, $CD21^+$, $CD8a^+$ NK subset and $CD163^-CD14^-$ cells, as analyzed by one-way ANOVA. Data are presented as mean values ± SEM, $n = 5$ [$n = 2$ (SWNT), $n = 3$ (SWNT-SHP1i)] from 5 biologically independent replicates. Source data are provided as a Source data file.

https://doi.org/10.1038/s41467-024-52005-1

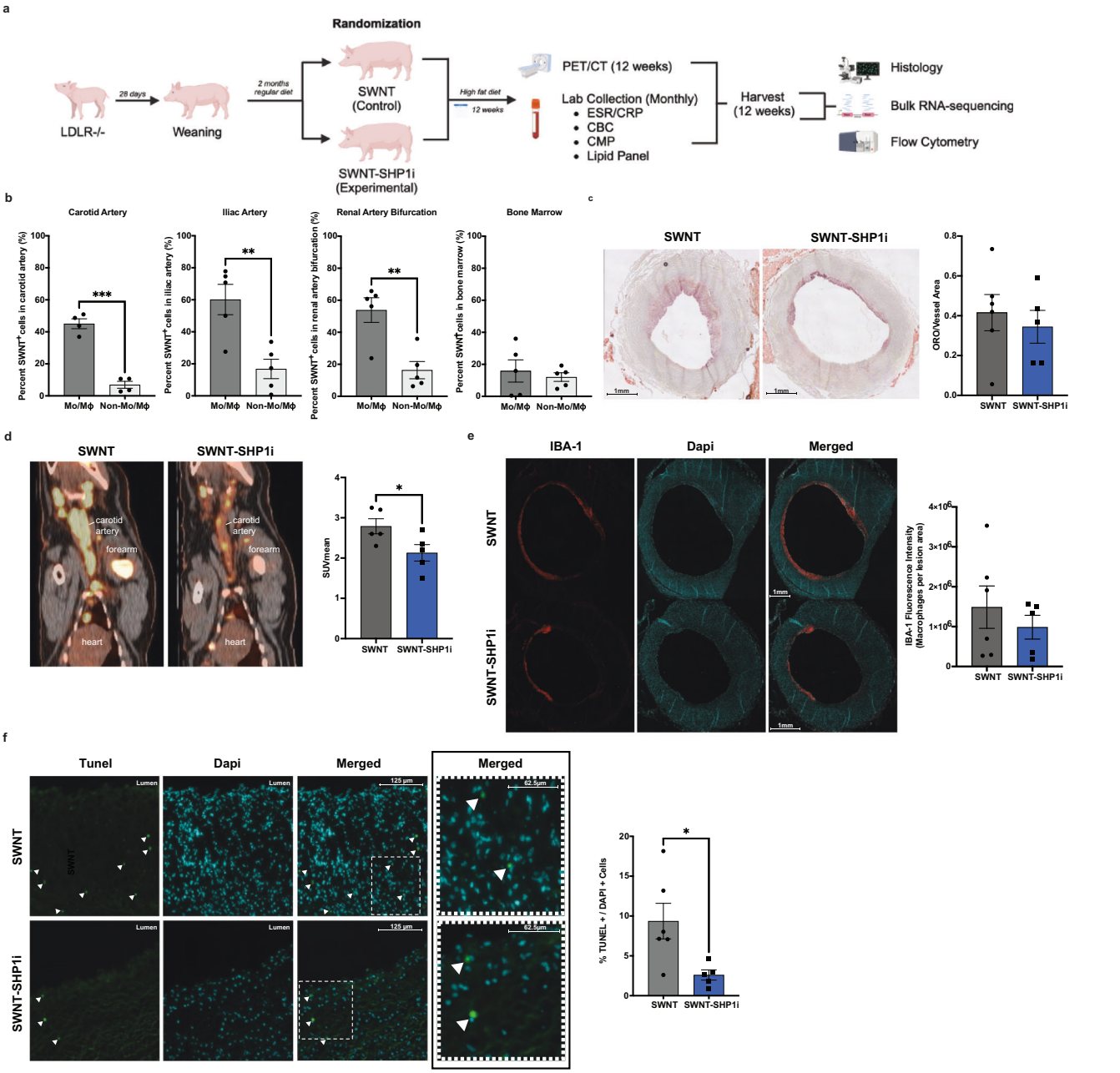


Fig. 3 | SWNTs accumulate in atherosclerotic plaque and SHP1 inhibition reduces both vascular inflammation and apoptotic cell accumulation in transgenic atherosclerotic pigs, in vivo. a Experimental workflow including downstream analyses. **b** Bar diagram of SWNT uptake in monocytes/macrophages versus non-monocytes/macrophages in multiple vascular beds of the pooled SWNT and SWNT-SHP1i treated pigs. MO stands for monocytes and MΦ stands for macrophages. SWNT/SWNT-SHP1i uptake by MO/MΦ was significantly higher than non-MO/MΦ in vascular beds including the carotid artery (***$p = 0.0001$), iliac artery (**$p = 0.0066$), and renal artery bifurcation (**$p = 0.0049$) as analyzed by an unpaired two-tailed t-test with Welch's correction. No significant difference was observed in SWNT/SWNT-SHP1i uptake by MO/MΦ compared to non-MO/MΦ in non-vascular tissue such as the bone marrow ($p = 0.6314$). Data are presented as mean values ± SEM. Carotid artery $n = 2$ (SWNT), $n = 2$ (SWNT-SHP1i); iliac artery $n = 2$ (SWNT), $n = 3$ (SWNT-SHP1i); renal artery bifurcation $n = 2$ (SWNT), $n = 3$ (SWNT-SHP1i); bone marrow $n = 2$ (SWNT), $n = 3$ (SWNT-SHP1i) over biologically independent samples. **c** Pigs treated with SWNT-SHP1i had similar atherosclerotic lesion sizes as SWNT controls in the RCA ostium ($p = 0.5763$). Data are presented as mean values ± SEM. $n = 6$ (SWNT) and $n = 5$ (SWNT-SHP1i) over 11 independent biological samples. **d** ^{18}F-FDG PET/CT imaging and analysis of the carotid arteries demonstrate that SWNT-SHP1i significantly reduces vascular inflammation. *$p = 0.0438$ by an unpaired two-tailed t-test with Welch's correction. Data are presented as mean values ± SEM. $n = 5$ (SWNT) and $n = 5$ (SWNT-SHP1i) over 10 independent biological samples. **e** In SWNT-SHP1i treated pigs, macrophage infiltration into the atherosclerotic lesion was not significantly lower than in SWNT controls ($p = 0.4339$). Data are presented as mean values ± SEM. $n = 6$ (SWNT) and $n = 5$ (SWNT-SHP1i) over 11 independent biological samples. **f** The RCA ostium of SWNT-SHP1i treated pigs contained significantly fewer TUNEL-positive apoptotic bodies compared to SWNT controls. *$p = 0.0280$ by unpaired two-tailed t-test with Welch's correction. Data are presented as mean values ± SEM. $n = 6$ (SWNT) and $n = 5$ (SWNT-SHP1i) over 11 independent biological samples. Source data are provided as a Source data file. Figure 3/panel a created with BioRender.com released under a Creative Commons Attribution-NonCommercial-NoDerivs 4.0 International license (https://creativecommons.org/licenses/by-nc-nd/4.0/deed.en).

https://doi.org/10.1038/s41467-024-52005-1

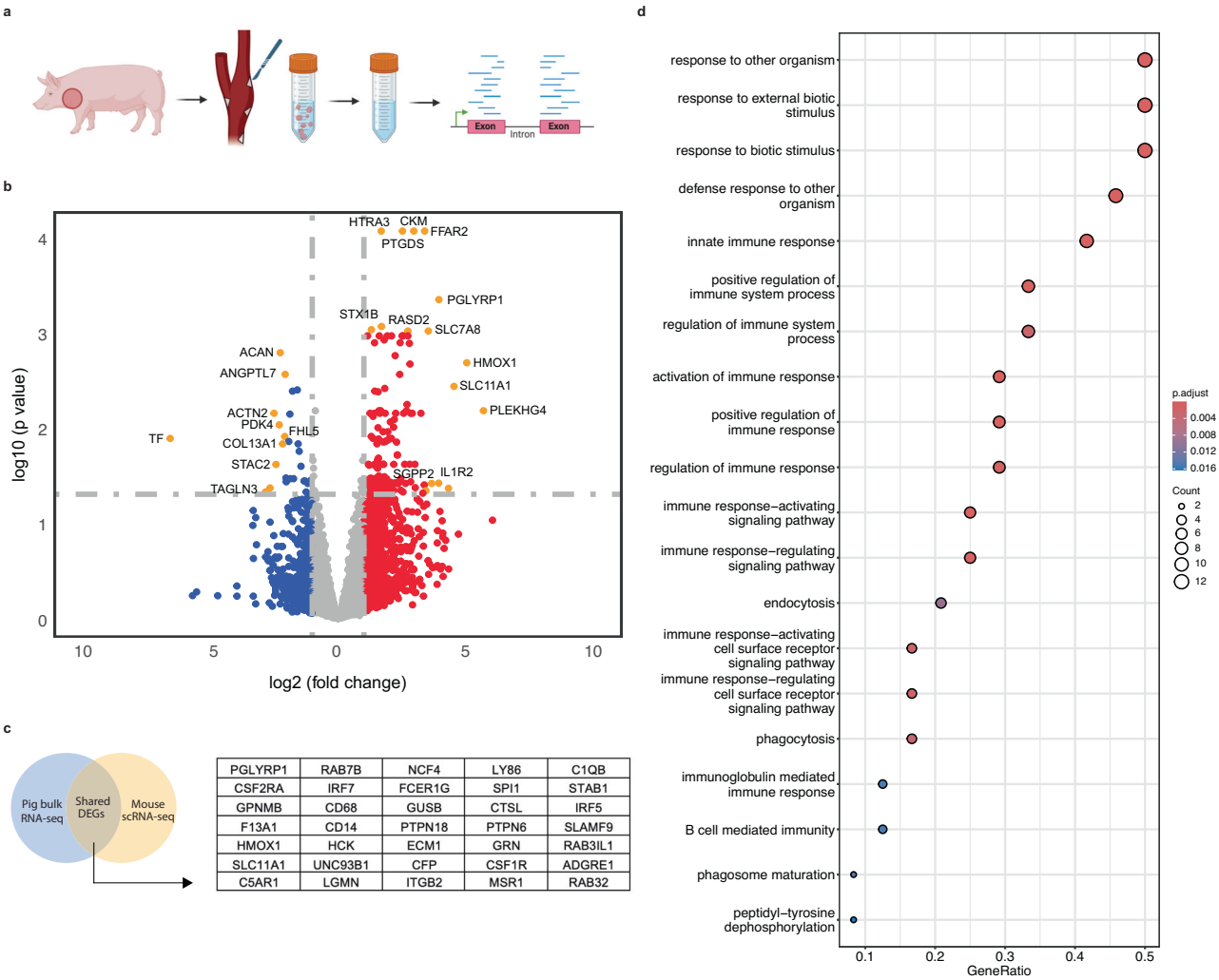


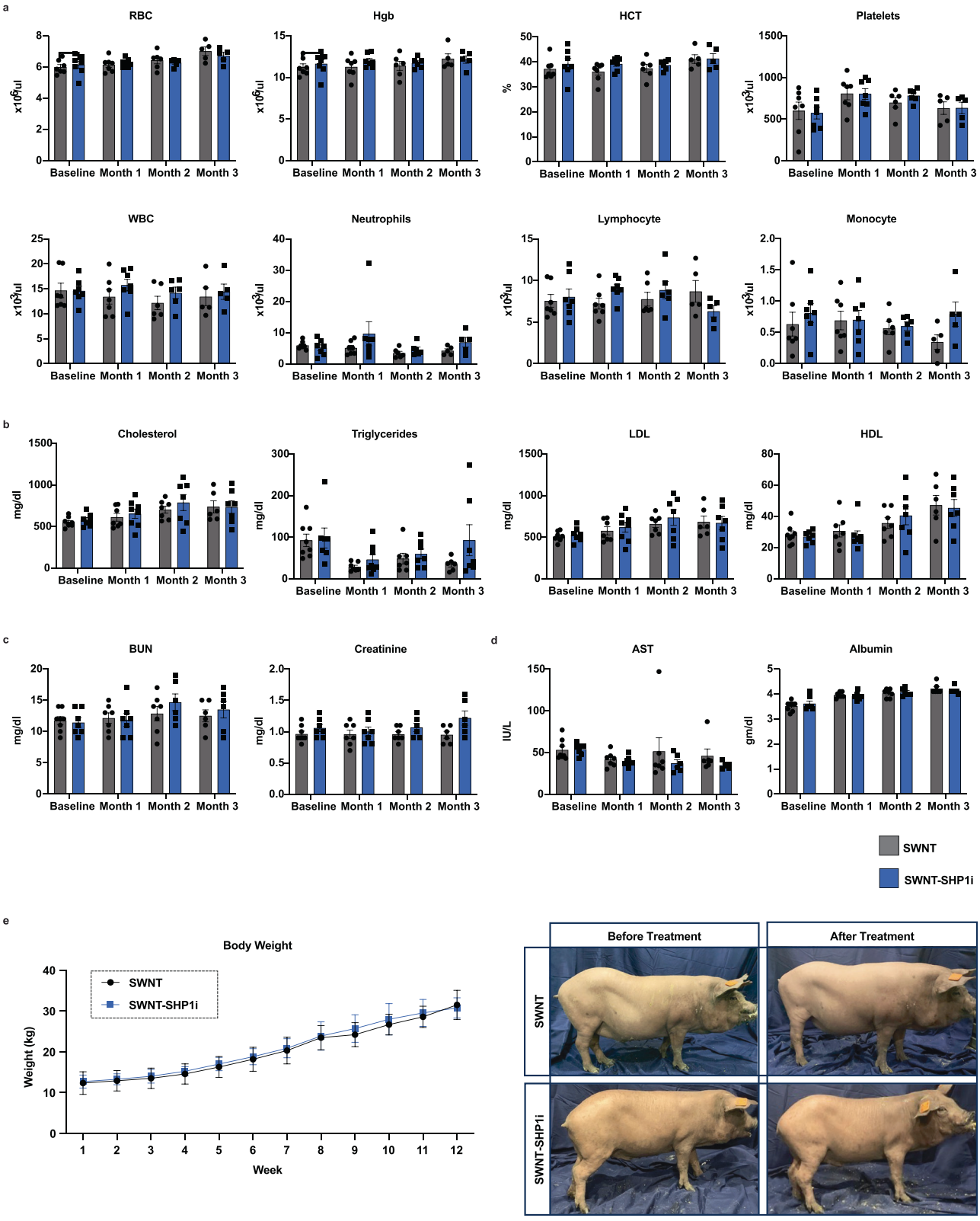
Fig. 4 | Pro-efferocytic therapies induce favorable immunological gene expression changes across species. a Bulk porcine RNA-sequencing experimental workflow. **b** Volcano plot of differentially expressed porcine genes from bulk RNA-sequencing in SWNT-SHP1i ($n = 3$) versus SWNT control ($n = 3$) common carotid arteries. Red and blue points represent up- and downregulated transcripts (log2 fold change >1 or <−1), respectively. Orange points indicate significantly differentially expressed genes, selected by log2 fold change (>2 or <−2) and adjusted p-value (<0.05, Benjamin–Hochberg correction). Gray points represent non-significant genes. Statistical significance was assessed using a likelihood ratio test (LRT) with two-sided testing. **c** Venn Diagram representing overlap of 35 significant differentially expressed genes between pig bulk RNA-sequencing results and published mouse scRNA-sequencing data from monocytes and macrophages. **d** Biological Process GO enrichment and pathway analysis of the 35 DEGs shared across species reveal pathways governing immune system response, response to an external biotic stimulus, endocytosis, and phagocytosis in the SWNT-SHP1i group. Adjusted p-value derived from the Benjamini & Hochberg test. Figure 4/panel a created with BioRender.com released under a Creative Commons Attribution-NonCommercial-NoDerivs 4.0 International license (https://creativecommons.org/licenses/by-nc-nd/4.0/deed.en).

Efferocytosis has recently emerged as a target for a wide range of fibrotic, malignant, infectious, and cardiovascular disorders[18–21]. A common theme across these conditions is the resistance of pathogenic cells to engulfment and removal by phagocytes, such as tumor-associated macrophages (TAM), lipid-laden foam cells, and other members of the innate immune system[6,18–21]. Investigators have begun to map the full repertoire of 'find me', 'eat me', and 'don't eat me' molecules which govern the 'edibility' of the target and the 'appetite' of the phagocyte as well as define how their expression becomes perturbed in disease[22]. More than a dozen candidate molecules have been validated in murine causation studies, and several drug development candidates have been prioritized for translation into humans[23]. This is particularly true in the field of immuno-oncology, where CD47 has been identified as a dominant anti-phagocytic signal that helps tumors evade immune surveillance[24]. Antibodies that block CD47 are now being tested in patients with leukemias, lymphomas, and a wide range of solid tumors[9,19,20]. There is hope that these agents may represent the first generation of macrophage-specific immunotherapy, and that this platform may complement the remarkable advances that have been observed with T cell-directed therapies over the last decade.

We recently found that cancer patients receiving anti-CD47 antibody therapy experience a potent reduction in vascular inflammation while their tumors are being treated[10]. These results motivated investigators to consider extending the use of pro-efferocytic therapies into cardiovascular patients, given prior results showing that reactivating the removal of apoptotic debris from the necrotic core can stabilize and even reverse murine atherosclerosis[6]. However, this approach may have an 'Achilles heel,' as patients with coronary artery disease may not tolerate the anemia (and resultant loss of oxygen carrying capacity) that occurs due to the erythrophagocytosis of red blood cells by indiscriminately activated splenic macrophages[9].

To overcome this translational hurdle, our group previously developed a pro-efferocytic 'Trojan horse' based on single-walled

https://doi.org/10.1038/s41467-024-52005-1



carbon nanotube technology[11,12,25]. These nanoparticles have several intrinsic benefits including their: 1. Documented biocompatibility[26,27]; 2. Ultra-high loading capacity[28]; and 3. Propensity to be preferentially scavenged and trafficked by inflammatory monocytes and macrophages[11,29]. We showed that SWNTs adorned with an inhibitor of SHP1—the anti-phagocytic phosphatase known to be downstream of CD47's receptor, SIRPα—could potently suppress vascular inflammation and prevent plaque progression in murine models of accelerated inflammation (apoE$^{-/-}$ mice with implanted subcutaneous angiotensin II infusion mini-pumps) and chronic atherosclerosis (apoE$^{-/-}$ mice fed a 'Western' diet)[12]. Unlike prior studies using systemic anti-CD47 therapies, these mice had no anemia or reticulocytosis, presumably because very little pro-phagocytic signal was delivered outside of the inflamed blood vessel due to SWNT selectivity[12].

Fig. 5 | Pro-efferocytic SWNTs do not induce the hematologic abnormalities associated with anti-CD47 Ab therapy. a Pigs treated with SWNT-SHP1i do not develop anemia or thrombocytopenia, with no significant difference in CBC lab values (WBC, neutrophils, lymphocyte, monocyte) between the SWNT and SWNT-SHP1i treated cohorts at each timepoint. Data are presented as mean values ± SEM. SWNT and SWNT-SHP1i cohort per group $n = 7$ (Baseline), $n = 7$ (Month 1), $n = 6$ (Month 2), $n = 5$ (Month 3) from independent biological samples. **b** SWNT-SHP1i was not significantly associated with derangements in lipid levels compared to SWNT controls. Data are presented as mean values ± SEM. SWNT cohort $n = 8$ (Baseline), $n = 7$ (Month 1), $n = 7$ (Month 2), $n = 6$ (Month 3); SWNT-SHP1i cohort $n = 7$ (Baseline), $n = 8$ (Month 1), $n = 7$ (Month 2), $n = 7$ (Month 3) from independent biological samples. **c**, **d** SWNT-SHP1i was not associated with derangements in **c** renal function, or **d** hepatic function compared to SWNT treated controls. Data are presented as mean values ± SEM. SWNT cohort $n = 8$ (Baseline), $n = 7$ (Month 1), $n = 7$ (Month 2), $n = 6$ (Month 3); SWNT-SHP1i cohort $n = 7$ (Baseline), $n = 7$ (Month 1), $n = 6$ (Month 2), $n = 6$ (Month 3) from independent biological samples. **e** There was no significant difference in body weight between SWNT and SWNT-SHP1i treated pigs. Data are presented as mean values ± SEM. SWNT cohort $n = 8$ (Weeks 1–3), $n = 7$ (Weeks 4–8), $n = 6$ (Weeks 9–11), $n = 3$ (Week 12); SWNT-SHP1i cohort $n = 7$ (Weeks 1–4), $n = 6$ (Weeks 5–11), $n = 4$ (Week 12) from independent biological samples. Source data are provided as a Source data file.

The current studies are therefore a key next step in the effort to advance targeted macrophage checkpoint inhibitors toward the cardiology clinic. Using an established large animal model of genetically-modified, atheroprone swine, we found that our SWNTs could be manufactured at scale (>1000 times the amounts needed for mouse studies and on the order of the amounts required for human applications), and that their ability to reduce vascular inflammation without inducing anemia was indeed preserved across species[12,30]. The significant reduction in carotid artery vascular inflammation, measured by ^{18}F-FDG PET/CT, after SWNT-SHP1i nanotherapy parallels our initial findings in mice[12] as well as in humans treated with anti-CD47 therapy[10]. Given the role of inflammation even at early stages of atherosclerosis pathogenesis[31], SWNT-SHP1i nanotherapy's effect on inflammation within the early atherosclerotic lesion highlights its therapeutic promise.

We further observed that SWNTs accumulate preferentially in the MO/MΦ compartment of early porcine atherosclerotic lesions, in contrast to non-vascular tissue beds such as the bone marrow (Fig. 3b). Despite no significant difference in fatty streak size, we observed a significant reduction in TUNEL staining with SHP1i nanotherapy (Fig. 3f), indicating removal of cells which otherwise would be destined to accumulate in the developing necrotic core.

By integrating RNA-sequencing results from mice and pigs, we sought to identify pathways that are consistently modulated by pro-efferocytic therapies across species as a way to better predict what might also occur in humans. While the list of significantly upregulated genes provides several insights regarding how inducing efferocytosis might favorably influence atherogenesis (Fig. 4c), it is interesting to note that HMOX1 is amongst the most potently induced factors. HMOX1 is thought to be antiatherogenic given its role as a rate limiting enzyme in heme catabolism[14–17]. Loss of HMOX1 expression in peritoneal macrophages significantly increases reactive oxygen species generation and the expression of proinflammatory cytokines, monocyte chemotactic protein-1(MCP-1), and interleukin 6 (IL-6)[17].

A literature review of the most highly upregulated DEGs highlights how SWNT-SHP1i nanotherapy may contribute to macrophage polarization, cell migration, and phagocytosis. Solute carrier 11A1 (SLC11A1/NRAMP1) is a divalent cation transporter that is found on late endosomes/lysosomes and proposed to contribute to phagosome maturation within the macrophage[32,33]. Another significantly upregulated DEG, Rab7b, is a small GTPase that interacts directly with Myosin II, and has been shown in in vitro experiments to regulate actin organization and cellular migration[34]. Furthermore, GPNMB has been shown to promote anti-inflammatory M2-like macrophage polarization in vitro, in part due to regulation of cytokine expression[35,36]. In the setting of acute kidney injury secondary to ischemia/reperfusion injury, GPNMB is mainly localized to and upregulated in M2-like macrophages within the kidney[35,36].

GO pathway analysis of these overlapping 35 DEGs demonstrated that genes involved in the positive regulation of the immune system were consistently activated in the blood vessel in response to SWNT-SHP1i nanotherapy. Upregulated pathways in the carotid arteries of SWNT-SHP1i treated pigs included immune system response, regulation of cytokine production, endocytosis, and phagocytosis. Given that the 'inflammatory hypothesis of atherosclerosis' is now almost universally accepted, it could be that the benefit of pro-efferocytic therapies is not solely driven by the physical removal of necrotic debris, but also by these unanticipated secondary benefits related to local cytokine suppression. In parallel, use of this cell-specific delivery nanotechnology to inflammatory macrophages may also potentially reduce risk of systemic immunosuppression.

This study has several limitations that warrant discussion. First, due to the prohibitive cost of synthesizing sufficient drug-conjugated SWNTs for aged pigs (which typically exceed 60–75 kg once mature[30]), we were only able to assess the impact of our therapy on early fatty streaks. Accordingly, additional randomized studies at later timepoints and with a larger number of pigs in each cohort will be necessary to confirm that SWNT-SHP1i can prevent enlargement of the established necrotic core, as has been demonstrated in mice. Furthermore, while ^{18}F-FDG PET/CT signal is commonly used as a surrogate of inflammation, it is important to recognize that this imaging modality is not specific for vascular disease, and may also reflect altered glucose uptake in the setting of infection, malignancy, and many other metabolic disorders[37].

While no hematological toxicity (or other organ dysfunction) was observed in response to therapy, some animals in both the SWNT and SWNT-SHP1i groups did expire during the study. Deaths occurred in both the SWNT ($n = 2$) and SWNT-SHP1i ($n = 1$) treated cohorts. Observations of breathing difficulties in one pig after anesthetic induction and before SWNT administration informed concerns that the deaths may have been in response to the sedation protocol. Once the isoflurane concentration and therapy infusion rate were reduced there were no episodes of respiratory depression or subsequent deaths. However, it will be important to further characterize the risks of SWNT administration before human studies can be initiated.

In conclusion, we show that pro-efferocytic, macrophage-selective nanoparticles can be generated at scale and successfully used to reduce vascular inflammation in a large animal model of atherosclerotic CVD. Because these nanoimmunotherapies circumvent the main limitation of systemic anti-CD47 antibodies (anemia), additional studies are indicated to confirm the tolerability and efficacy in longer-term models bearing higher plaque burdens. Ultimately, these efforts could lead to the introduction of 'Trojan horse' therapies that deliver a high concentration of drug to the inflamed blood vessel, without inducing off-target toxicity elsewhere in the body.

Methods

'Large batch' SWNT synthesis

We generated monocyte-selective pro-phagocytic nanoparticles as previously described, with several key modifications[11,12]. These modifications were necessary to allow the scaling required to generate sufficient nanoparticles for ~70 kg pigs, instead of the ~25 g mice tested previously[11,12]. Briefly, 300 mg HiPco (high-pressure carbon mono oxide) RAW single-walled carbon nanotubes (SWNTs) (Nanointegris) and 300 mg DSPE-050PA (NOF Corporation) were added into 100 mL DDI water, sonicated in a large ultrasonic bath (Fisher Scientific,

CPX2800) under ice bath for ~12 h, then centrifuged at 100,000 × *g* and 4 °C for 2 h (Thermo Scientific, Sorvall WX + Ultra series) to obtain PEGylated SWNTs. Unbound lipid was washed away with multiple rounds of PBS using 100 kDa centrifugal filters (Millipore) at 4000 rpm and 4 °C.

Because of the prohibitive expense of adding molecular imaging probes in a large animal study, the Cy5.5 fluorophore used in prior studies was omitted from the nanoparticles used throughout most of the current study. However, in limited experiments, Cy5.5 was conjugated to SWNTs. To conjugate Cy5.5 Mono NHS Ester (GE Life Sciences) to SWNT-PEG, Cy5.5-Mono NHS Ester was dissolved in DMSO and then incubated with SWNT-PEG solution at pH of ~8.1 overnight. Excess Cy5.5 was removed by centrifugal filtration (MWCO: 100 KDa) to obtain purified SWNT-Cy5.5. SWNT concentrations were quantified by Nanodrop (Thermo Scientific, Nanodrop One) with an extinction coefficient of 7.9×10^6 M^{-1} cm^{-1} at 808 nm. The size and zeta potential were measured by Zetasizer (Malvern).

SWNTs were then loaded with a small molecule inhibitor of SHP-1 (SHP1i) (Millipore Corp., NSC-87877), which is the intracellular anti-phagocytic effector phosphatase downstream of CD47's receptor, SIRP-α[18]. To load SHP1i onto SWNTs, SHP1i powder was dissolved in DDI water and added to stirred SWNTs (pH = 7.4) at room temperature overnight to form SWNT-SHP1i. Unbound SHP1i was washed away with PBS using 100 kDa centrifugal filters (Millipore) at 4000 rpm. The concentration of loaded SHP1i was measured using a Nanodrop at its absorption of 320 nm with the standard curve shown in Fig. S1a in the ESM. The size and ζ-potential of SWNT-SHP1i were measured by Zetasizer (Malvern).

Physiochemical SWNT characterization

UV-Vis spectroscopy and FT-IR spectroscopy analysis. UV-Vis spectroscopy (200–800 nm) was performed for SHP1i, SWNT, and SWNT-Cy5.5-SHP1i using the Nanodrop 2000 (2 μL per sample for each test). FT-IR spectroscopy (Mattson Research) in the 500–4500 cm^{-1} regime was performed for SHP1i, SWNT, and SWNT-Cy5.5-SHP1i. KBr circular discs (International Crystal Laboratories) were used to hold the samples.

SHP1i release assay. We evaluated pH-dependent SHP1i release from SWNTs in PBS buffer (pH 7.4 and 6.5). SWNT-SHP1i was added to a MINI Dialysis Device (MWCO: 20 K). At fixed timepoints from 10 min to 48 h, 2 μL of the release media (from a 'sink' of 3 mL) was removed to test the release rate of SHP1i via Nanodrop. The cumulative drug release (CDR) percentage was calculated by the following equation and the SHP1i standard curve in Fig. S1a in the ESM:

$$CDR\ (\%) = W_{released}/W_{loaded} \times 100\%$$

Here, CDR represents the cumulative drug release percentage, $W_{released}$ represents the mass of released SHP1i in the release media, and W_{loaded} represents the total mass of SHP1i loaded on SWNT.

Efferocytosis assay. Briefly, 2×10^6 RAW264.7 macrophages were plated in DMEM/10% FBS overnight to be used as phagocytes and target cells. RAW(phagocyte) cells were then co-cultured with 4 nM SWNT or SWNT-SHP1i (9 μL 50 mM SHP1i loaded in 3 mL 400 nM SWNT) at 37 °C for 48 h. On day three, RAW(target) cells were treated with STS (1 μM) for 4 h to induce apoptosis. RAW(phagocyte) cells were washed with PBS and 1×10^5 cells were plated in a 48-well plate (Corning). In parallel, RAW(target) cells were centrifuged at 300 × *g* and resuspended in 5 mL of Incucyte pHrodo wash buffer (Sartorius, 4659). Cells were centrifuged at 300 × *g* and resuspended in Incucyte pHrodo labeling buffer (Sartorius, 4658) at a density of 1×10^6 cells/mL. 1 μL/mL of pH sensitive pHrodo Orange Cell Labeling Dye (Sartorius, 0051) was mixed into the RAW (target) cell and labeling buffer solution and left to incubate at 37 °C for 1 h. Cells were harvested by centrifugation, washed twice, and resuspended in DMEM/10% FBS media. 2×10^5 RAW (target) cells/well were added to the 48-well plate to create a 2:1 ratio of target: phagocyte RAW cells. The plate was then placed in an Incucyte machine (Sartorius). The Incucyte detects a pH drop and corresponding fluorescence increase (Emission max: 605 nm) when the labeled RAW(target) cells are within the acidic lysosome of the RAW(phagocyte) cells. The fluorescence intensity of SWNT treated ($n = 16$) and SWNT-SHP1i treated ($n = 16$) wells were measured every hour for 24 h (Incucyte).

Large animal atherosclerosis studies

Experimental animals. The Yucatan miniature pigs utilized in this study were obtained from Exemplar Genetics, IA, USA. These animals were originally generated by introducing a loss of function mutation in exon 4 of the LDLR gene, a common site of mutation in patients with familial hypercholesterolemia, as previously described[30]. Litters of $LDLR^{-/-}$ and control $LDLR^{+/+}$ animals were generated via somatic cell nuclear transfer (cloning), weaned at 28 days of age, and transitioned to a general swine diet for two months. Pigs were then transitioned to a high fat/high calorie Western diet and randomized to SWNT control ($n = 8$) and SWNT-SHP1i experimental ($n = 8$) treatment groups. Pigs were maintained on the high fat diet for 12 weeks. Each week, pigs were placed under general anesthesia and 400 nM of SWNT or SWNT-SHP1i was infused intravenously for ~15–30 min with close monitoring of vitals and body temperature. Animal weights were obtained weekly. Monthly blood draws were collected for CBC, CMP, and lipid panel studies. Before euthanasia in week 12, a PET-CT (Discovery MI, GE Healthcare, Chicago, Il) scan was performed to measure vascular inflammation in a randomly selected cohort of 10 animals. After sacrifice, pig blood and tissue samples were sent for histology, bulk RNA-sequencing, and flow cytometry analysis to evaluate therapeutic efficacy and safety endpoints. Both male ($n = 12$) and female ($n = 4$) pigs were bred for, randomized, and included in this study. Sex-based sub-analysis was not performed due to the baseline sample size in the SWNT and SWNT-SHP1i treated cohorts.

Animals were generated and housed at Exemplar Genetics (Sioux Center, IA) and all experiments were conducted with local APLAC approval (33951). Exemplar Genetics has PHS assurance (A4579-01), USDA research registration (42R 0044) and Class B Dealer registration (42 B 0270). Euthanasia was performed using pharmaceutical grade commercial euthanasia solution injected at a minimum dose of 1 mL per 5 kg weight plus 1 mL. After completion, methods of confirmation of euthanasia included bilateral thoracotomy and harvesting of vital tissues.

Processing and staining of pig blood samples for flow cytometry. One mL of pig blood was incubated with 10 mL of 1X RBC lysis buffer (BD Pharm Lyse, BD Biosciences, 555899) for 10 min. Thereafter, 30 mL of FACS buffer (PBS with 2% FBS and 2 mM EDTA) was added and the sample was centrifuged at 500 × *g* for 5 min. The cell pellet was then resuspended into FACS buffer and incubated with human BD Fc block (BD Pharmingen, 564220) for 20 min and subsequently incubated with various surface antibodies (including PE-conjugated anti-pig CD163 (Bio-RAD, MCA2311PE), FITC-conjugated anti-pig CD14 (BIO-RAD, MCA1218F), Alexa Fluor 647 conjugated anti-pig CD8a (BD Pharmingen, 561475), pacific blue conjugated anti-pig CD3 (BIO-RAD, MCA5951PB), PE-Cy7 conjugated anti-human CD21 with pig reactivity (BD Pharmingen, 561374)) for 20 min. Samples were washed with 4 mL of FACS buffer and fixed with 0.5 mL of 4% paraformaldehyde (Thermo Scientific) for 15 min and again washed with 4 mL of FACS buffer. Afterward, samples were washed twice with 1X permeabilization buffer (Invitrogen, 00-8333-56) and incubated with anti-PEG antibody (EMD Millipore Corp., MABS1964-100UG) for 30 min, washed with the same buffer, and incubated with BV711 conjugated secondary antibody (Biolegend, 406539) for 30 min. All incubations were done at 4 °C. Samples were then washed with 1X permeabilization buffer,

resuspended into FACS buffer, and analyzed on a Cytek Aurora flow cytometer (Cytek Biosciences) using SpectroFlo software.

Gating strategy for SWNT uptake in circulating immune cells. Intact singlet cells were identified and gated to label different immune cell populations. $CD3^+$ and $CD21^+$ cells, which represent porcine T cells and B cells, respectively, were gated in the singlet population and the remaining cells (excluding $CD3^+$ and $CD21^+$ cells) were termed $CD3^-CD21^-$ cells. Thereafter, $CD3^-CD21^-$ cells were gated for the $CD8a^+$ NK subset. The remaining cells were termed $CD3^-CD21^-CD8a^-$ and further gated for different subsets of monocytes. A quadrant gate was applied on $CD3^-CD21^-CD8a^-$ cells based on CD163 and CD14 antibody staining. $CD163^+CD14^-$, $CD163^+CD14^+$, and $CD163^-CD14^+$ cells reflect distinct monocyte populations. In contrast, $CD163^-CD14^-$ cells were deemed to represent all other cell types, excluding the immune cell types described above.

The $SWNT^+$ gate for each circulating cell type was set using blood from untreated pigs. These baseline samples from animals, which were never exposed to SWNTs, were processed, stained, and recorded on the flow cytometer using our staining panels, with appropriate compensation controls. Any signal suggesting staining with the anti-PEG antibody (which defines the presence of SWNTs) in these untreated samples was considered to be background staining, and defined as zero, with gates set accordingly. Thereafter, any positive signal in the treated animals was deemed to reflect $SWNT^+$ cells. The remaining cells were defined as $SWNT^-$ cells.

Dissociating and staining arterial samples for flow cytometry. After sacrifice, fresh carotid artery, iliac artery, and renal artery bifurcation tissue was washed thrice with RPMI with 3% fetal bovine serum containing Benzonase Nuclease (Millipore Sigma, 9025-65-4, 10 μL per/100 mL media, medium A) to remove blood. Thereafter, the tissue was mechanically dissociated by chopping/slicing using scissors and a razor blade. The tissue was then spun down for 5 min at 500 × *g*, and the supernatant was aspirated. The tissue was resuspended in 0.25% of Collagenase-I solution (Thermo Scientific, J62406.MC) containing Collagenase XI at 1000 U/mL (Millipore Sigma, 9001-12-1) and Hyaluronidase-I at 600 U/mL (Millipore Sigma, 37326-33-3) and incubated at 37 °C for 40 min. Samples of tissue were vortexed 3 times during incubation. Samples were washed with RPMI with 3% fetal bovine serum containing Benzonase Nuclease (10 μL per/100 mL media) and 5 mM EDTA (medium B), resuspended into the same medium, and filtered through 70 μm mesh to obtain a single-cell suspension. Afterward, RBC lysis was done using ACK lysis buffer (Gibco, A10492-01), then washed with medium B and resuspended in FACS buffer.

Samples were subsequently incubated with human BD Fc block (BD Pharmingen, 564220) for 20 min and then incubated with viability dye (blue-fluorescent reactive dye, Invitrogen, L34961A) and various surface marker antibodies (including PE-conjugated anti-pig CD163 (Bio-RAD, MCA2311PE), FITC-conjugated anti-pig CD14 (BIO-RAD, MCA1218F), Alexa Fluor 647 conjugated anti-pig CD8a (BD Pharmingen, 561475), pacific blue conjugated anti-pig CD3 (BIO-RAD, MCA5951PB), PE-Cy7 conjugated anti-human CD21 with pig reactivity (BD Pharmingen, 561374)) for 20 min. Samples were washed with 4 mL of FACS buffer and fixed with 0.5 mL of 4% paraformaldehyde (Thermo Scientific) for 15 min and again washed with 4 mL of FACS buffer. Afterward, samples were washed twice with 1X permeabilization buffer (Invitrogen, 00-8333-56) and incubated with anti-PEG antibody (EMD Millipore Corp., MABS1964-100UG/Invitrogen, MA5-24693) for 30 min, washed with the same buffer, and incubated with BV711 conjugated secondary antibody (Biolegend, 406539)/Alexa Fluor 790 conjugated secondary antibody (Invitrogen, A11369) for 30 min. All incubations were done at 4 °C. Samples were then washed with 1X permeabilization buffer, resuspended into FACS buffer, and analyzed on Cytek Aurora flow cytometer (Cytek Biosciences, Inc., Model:5L) using SpectroFlo software.

Positioning of $SWNT^+$ gates for tissue samples. The $SWNT^+$ gate for each tissue cell type was set using a fluorescence minus one (FMO) control, in which every fluorophore except the anti-PEG antibody was used. Background fluorescence in the FMO was considered zero, with gates set accordingly. Thereafter, positive signal was deemed to reflect a $SWNT^+$ cell.

Processing and staining bone marrow cells for flow cytometry. After sacrifice, fresh bone marrow was flushed with saline to extract marrow cells. The cells were then filtered through a 70 μm mesh to remove spicules and obtain a single-cell suspension. Afterward, RBC lysis was performed using ACK lysis buffer (Gibco, A10492-01). Cells were then resuspended into FACS buffer, stained using the antibody panel described above, and analyzed on a Cytek Aurora flow cytometer using SpectroFlo software.

PET/CT. ^{18}F-FDG PET/CT imaging was performed to measure changes in vascular inflammation within the atherosclerotic carotid artery in response to treatment with SWNT-SHP1i ($n = 5$) or control SWNT ($n = 5$) at the University of Iowa Institute for Biomedical Imaging (IIBI). Pigs were fasted for 12 hours prior to imaging and glucose was measured to mitigate any confounding effects of physiologic glucose processing after food. Pigs underwent isoflurane anesthetic induction and were maintained under anesthesia until completion of scan. Heart rate, oxygen saturation, respiratory rate and body temperature were monitored and maintained during the imaging session. ^{18}F-FDG bolus (460.1 MBq +/− 81.42) was administered by peripheral IV via ear vein. After a 60-min uptake period, each pig was moved to the scanner room and placed prone on the PET/CT scanner bed (Discovery MI, GE Healthcare, Chicago, Il). A 20-min single bed list mode PET scan was acquired with the thoracic region in the field of view (FOV), followed by a CT for anatomical co-registration and attenuation correction. List mode data was reconstructed with the GE Discovery MI scanner software. Animal imaging at the University of Iowa IIBI was reviewed and approved by the University of Iowa Animal Care and Use Committee.

Using Inveon Research Workplace (IRW) software (Siemens Medical Solutions, Knoxville, TN), region-of-interest analysis (ROI) was performed to quantify ^{18}F-FDG uptake in the right and left carotid artery, respectively. Pig identification and cohort assignment were blinded for this analysis. The three-dimensional ROI of the right and left carotid artery bifurcation (extending from the proximal common carotid artery into the proximal internal and external carotid arteries) was outlined using coronal slices from the CT scan. Standardized minimum and maximum target image presets and threshold range were applied to the image datasets. ROI results were reported as standard uptake values (SUV) and the analysis process was repeated for each pig. The left and right carotid artery SUV_{mean} values were averaged for analysis.

Tissue preparation for immunohistochemical analysis. Porcine vascular tissue was perfusion-fixed with phosphate-buffered paraformaldehyde (4%) immediately after sacrifice. The right coronary artery ostium (RCA-O) was dehydrated in 15% and 30% sucrose for 24 h each and then embedded in OCT blocks. The RCA-O was sectioned at 7 μM thickness starting from the proximal to distal end of the vessel. For Oil Red O (ORO) analysis, 3 serial RCA-O sections at 100 μm intervals (0–200 μm) were collected from each pig for staining. Images were blinded for quantitative analysis. Lesion area was demarcated as the total ORO positive area and was normalized to the total vessel area calculated by encircling the RCA-O vessel lumen.

To assess macrophage infiltration into the early atherosclerotic lesion, sections were stained for IBA-1 (FUJIFILM Wako Chemicals;

1:500) and followed by Alexa Fluor 555 goat anti-rabbit (Invitrogen; 1:250). Fluorescence intensity was quantified using ImageJ Software and normalized to vessel area measured from a serial section. TUNEL Assay (Roche, 11684795910) was performed on RCA-O sections to quantify the number of apoptotic cells. ImageJ software was used to set a standard threshold for positive signal. TUNEL$^+$ cell number in the lesion was divided by total cell number (DAPI$^+$) in the lesion. ORO, IBA-1, and TUNEL staining were performed on all available vascular tissue from SWNT and SWNT-SHP1i treated pigs.

Carotid artery preparation for bulk RNA-sequencing. Flash-frozen carotid arteries of pigs treated with either SWNT (n = 3) or SWNT-SHP1i (n = 4) were harvested. First, the tissue was dissected free from perivascular adipose and connective tissue, then random sections of the common carotid artery were isolated from each pig. RNA was extracted using Trizol reagent (Life Technologies, 15596018), and subsequently sent for Bulk RNA-sequencing.

Bulk RNA-sequencing and data analysis. For the assessment of RNA-seq data quality, per base sequence quality plots were analyzed using FastQC. TrimGalore was employed for the trimming of sequence reads. Subsequently, the RNA-seq reads were aligned to the pig genome (Sscrofa11.1) using the STAR software[38]. Reads aligning to exon coordinates were quantified using RSEM and featurecounts[39]. Raw read counts were subjected to variance stabilizing transformation (VST) using the DESeq2 R package[40]. Normalized expressions were calculated by determining the mean and standard deviations for each gene. Z-scores were computed by subtracting the mean from each expression value and dividing by the standard deviation. PCA was performed on the data to assess sample clustering and identify potential outliers. Based on PCA results, sample B9100C was identified as an outlier and subsequently removed from further analysis. Differential expression genes (DEGs) between different groups were identified using the DESeq2 R package, employing a likelihood ratio test (LRT) with two-sided testing[40]. Significance was determined based on genes with a Benjamin–Hochberg corrected p-value < 0.05 for multiple comparisons. Volcano plots illustrating differential expression were created using the ggplot2 R package[41].

Pathway analysis. Significant DEGs (p adj. <0.05) from the pig bulk RNA-Seq were inputted into the gene ontology (GO) knowledgebase to identify functions and pathways associated with the DEGs[42–44]. In order to integrate the pig bulk RNA-seq data with the previously published murine single-cell RNA-seq[12], cluster 1&4 DEGs (representing the macrophage and monocyte subpopulations, respectively) were filtered to create a separate table. Shared DEGs were identified using excel to highlight duplicate gene names included in both the pig bulk RNA-seq and mouse scRNA-seq (clusters 1&4) lists. DEGs were then inputted into the PANTHER Pathway for GO term enrichment analysis to allow for the identification of conserved pathways in both porcine and murine models[44]. Subsequently, the GO pathway enrichment analyses of DEGs and shared DEGs in the key modules were performed by the R package clusterProfiler[45].

Safety studies. To evaluate safety, laboratory studies were obtained monthly at the time of infusion and included complete blood counts with differential, complete metabolic panels, and lipid panels. Body weight was measured at weekly treatment infusions. Blood pressure was similarly obtained and monitored at the time of the SWNT or SWNT-SHP1i infusion.

Statistical analysis. Groups were compared using either the unpaired two-tailed t-test, with or without Welch's correction, or one-way ANOVA. Welch's test was performed for normally distributed samples with unequal standard deviations. One-way ANOVA was used for comparison of more than two groups, and Kaplan–Meier method was applied for survival analysis. A P value < 0.05 criteria was used to indicate statistical significance and graphs represent the mean of each data set with error bars denoting standard error. Measurements for the flow cytometry, ^{18}F-FDG PET/CT, histology, and bulk RNA-Seq analysis represent distinct samples. Measurements for the lab values reflect repeated measurements at monthly timepoints. GraphPad Prism 8-9 (GraphPad Inc.) was used to perform all statistical analyses.

Reporting summary

Further information on research design is available in the Nature Portfolio Reporting Summary linked to this article.

Data availability

The bulk RNA-seq data generated in this study have been deposited in the GEO database under accession code GSE270259. Source data are provided with this paper.

References

1. Arnett D. K. et al. 2019 ACC/AHA Guideline on the Primary Prevention of Cardiovascular Disease: Executive Summary: A Report of the American College of Cardiology/American Heart Association Task Force on Clinical Practice Guidelines. *J. Am. Coll. Cardiol.* **74**, 1376–1414 (2019).
2. Tsao C. W. et al. Heart Disease and Stroke Statistics—2022 Update: A Report From the American Heart Association. *Circulation* **145**, e153-e639 (2022).
3. Ridker, P. M. et al. Antiinflammatory therapy with canakinumab for atherosclerotic disease. *N. Engl. J. Med.* **377**, 1119–1131 (2017).
4. Adkar, S. S. & Leeper, N. J. Efferocytosis in atherosclerosis. *Nat. Rev. Cardiol.* https://doi.org/10.1038/s41569-024-01037-7 (2024)
5. Arandjelovic, S. & Ravichandran, K. S. Phagocytosis of apoptotic cells in homeostasis. *Nat. Immunol.* **16**, 907–917 (2015).
6. Kojima, Y. et al. CD47-blocking antibodies restore phagocytosis and prevent atherosclerosis. *Nature* **536**, 86–90 (2016).
7. Libby, P. et al. Atherosclerosis. *Nat. Rev. Dis. Prim.* **5**, 56 (2019).
8. Li, M. et al. Programmed cell death in atherosclerosis and vascular calcification. *Cell Death Dis.* **13**, 467 (2022).
9. Advani, R. et al. CD47 blockade by Hu5F9-G4 and rituximab in non-Hodgkin's lymphoma. *N. Engl. J. Med.* **379**, 1711–1721 (2018).
10. Jarr, K. U. et al. Effect of CD47 Blockade on Vascular Inflammation. *N. Engl. J. Med.* **384**, 382–383 (2021).
11. Smith, B. R. et al. Selective uptake of single-walled carbon nanotubes by circulating monocytes for enhanced tumour delivery. *Nat. Nanotechnol.* **9**, 481–487 (2014).
12. Flores, A. M. et al. Pro-efferocytic nanoparticles are specifically taken up by lesional macrophages and prevent atherosclerosis. *Nat. Nanotechnol.* **15**, 154–161 (2020).
13. Zhang, Y. et al. Macrophage-targeted single walled carbon nanotubes stimulate phagocytosis via pH-dependent drug release. *Nano Res.* **14**, 762–769 (2021).
14. Ishikawa, K. et al. Heme oxygenase-1 inhibits atherogenesis in Watanabe heritable hyperlipidemic rabbits. *Circulation* **104**, 1831–1836 (2001).
15. Ishikawa, K. et al. Heme oxygenase-1 inhibits atherosclerotic lesion formation in lDL-receptor knockout mice. *Circ. Res.* **88**, 506–512 (2001).
16. Juan, S. H. et al. Adenovirus-mediated heme oxygenase-1 gene transfer inhibits the development of atherosclerosis in apolipoprotein E-deficient mice. *Circulation* **104**, 1519–1525 (2001).
17. Orozco, L. D. et al. Heme oxygenase-1 expression in macrophages plays a beneficial role in atherosclerosis. *Circ. Res.* **100**, 1703–1711 (2007).

18. Jarr, K. U., Kojima, Y., Weissman, I. L. & Leeper, N. J. 2021 Jeffrey M. Hoeg Award Lecture: defining the role of efferocytosis in cardiovascular disease: a focus on the CD47 (cluster of differentiation 47) axis. *Arterioscler Thromb. Vasc. Biol.* **42**, e145–e154 (2022).
19. Majeti, R. et al. CD47 is an adverse prognostic factor and therapeutic antibody target on human acute myeloid leukemia stem cells. *Cell* **138**, 286–299 (2009).
20. Willingham, S. B. et al. The CD47-signal regulatory protein alpha (SIRPa) interaction is a therapeutic target for human solid tumors. *Proc. Natl Acad. Sci. USA* **109**, 6662–6667 (2012).
21. Doran, A. C., Yurdagul, A. Jr. & Tabas, I. Efferocytosis in health and disease. *Nat. Rev. Immunol.* **20**, 254–267 (2020).
22. Park, S. Y. & Kim, I. S. Engulfment signals and the phagocytic machinery for apoptotic cell clearance. *Exp. Mol. Med.* **49**, e331 (2017).
23. Mehrotra, P. & Ravichandran, K. S. Drugging the efferocytosis process: concepts and opportunities. *Nat. Rev. Drug Discov.* **21**, 601–620 (2022).
24. Chao, M. P., Weissman, I. L. & Majeti, R. The CD47-SIRPα pathway in cancer immune evasion and potential therapeutic implications. *Curr. Opin. Immunol.* **24**, 225–232 (2012).
25. Smith, B. R. & Edelman, E. R. Nanomedicines for cardiovascular disease. *Nat. Cardiovasc. Res.* **2**, 351–367 (2023).
26. Liu, Z. et al. Circulation and long-term fate of functionalized, biocompatible single-walled carbon nanotubes in mice probed by Raman spectroscopy. *Proc. Natl Acad. Sci. USA* **105**, 1410–1415 (2008).
27. Schipper, M. L. et al. A pilot toxicology study of single-walled carbon nanotubes in a small sample of mice. *Nat. Nanotechnol.* **3**, 216–221 (2008).
28. Liu, Z., Sun, X., Nakayama-Ratchford, N. & Dai, H. Supramolecular chemistry on water-soluble carbon nanotubes for drug loading and delivery. *ACS Nano* **1**, 50–56 (2007).
29. Flores, A. M. et al. Nanoparticle therapy for vascular diseases. *Arterioscler Thromb. Vasc. Biol.* **39**, 635–646 (2019).
30. Davis B. T. et al. Targeted disruption of LDLR causes hypercholesterolemia and atherosclerosis in Yucatan miniature pigs. *PLoS One* **9**, e93457 (2014).
31. Soehnlein, O. & Libby, P. Targeting inflammation in atherosclerosis—from experimental insights to the clinic. *Nat. Rev. Drug Discov.* **20**, 589–610 (2021).
32. Cellier, M. F., Courville, P. & Campion, C. Nramp1 phagocyte intracellular metal withdrawal defense. *Microbes Infect.* **9**, 1662–1670 (2007).
33. Blackwell, J. M., Searle, S., Goswami, T. & Miller, E. N. Understanding the multiple functions of Nramp1. *Microbes Infect.* **2**, 317–321 (2000).
34. Borg, M., Bakke, O. & Progida, C. A novel interaction between Rab7b and actomyosin reveals a dual role in intracellular transport and cell migration. *J. Cell Sci.* **127**, 4927–4939 (2014).
35. Yu, B., Sondag, G. R., Malcuit, C., Kim, M. H. & Safadi, F. F. Macrophage-associated osteoactivin/GPNMB mediates mesenchymal stem cell survival, proliferation, and migration via a CD44-dependent mechanism. *J. Cell Biochem.* **117**, 1511–1521 (2016).
36. Zhou, L. et al. Glycoprotein non-metastatic melanoma protein b (Gpnmb) is highly expressed in macrophages of acute injured kidney and promotes M2 macrophages polarization. *Cell Immunol.* **316**, 53–60 (2017).
37. Vaidyanathan, S., Patel, C. N., Scarsbrook, A. F. & Chowdhury, F. U. FDG PET/CT in infection and inflammation-current and emerging clinical applications. *Clin. Radio.* **70**, 787–800 (2015).
38. Dobin, A. et al. STAR: ultrafast universal RNA-seq aligner. *Bioinformatics* **29**, 15–21 (2013).
39. Li, B. & Dewey, C. N. RSEM: accurate transcript quantification from RNA-Seq data with or without a reference genome. *BMC Bioinformatics* **12**, 323 (2011).
40. Love, M. I., Huber, W. & Anders, S. Moderated estimation of fold change and dispersion for RNA-seq data with DESeq2. *Genome Biol* **15**, 550 (2014).
41. Wickham, H. ggplot2: Elegant Graphics for Data Analysis. *Springer-Verlag*. Retrieved from https://ggplot2.tidyverse.org (2016).
42. Ashburner, M. et al. Gene ontology: tool for the unification of biology. *Nat Genet.* **25**, 25–29 (2000).
43. Gene Ontology Consortium et al. The Gene Ontology knowledgebase in 2023. *Genetics* **224**, (2023).
44. Thomas, P. D. et al. PANTHER: Making genome-scale phylogenetics accessible to all. *Protein science : a publication of the Protein Society* **31**, 8–22 (2022).
45. Wu, T. et al. clusterProfiler 4.0: A universal enrichment tool for interpreting omics data. *Innovation (Cambridge (Mass.))* **2**, 100141 (2021).

Acknowledgements

This work was supported by the Falk Foundation (Dr. Ralph and Marian Falk Medical Research Trust Transformational Award to N.J.L.), National Institutes of Health (R35 HL144475 to N.J.L.), the American Heart Association (EIA34770065 to N.J.L.; 18TPA34230113 to B.R.S.), the National Institutes of Health (R01CA244491 to B.R.S.), the Greathouse Family Foundation (to N.J.L.), Perkin-Elmer Post-doctoral Fellowship (to Y.Z.), and the Sarnoff Cardiovascular Research Foundation (to S.B.). We also acknowledge Exemplar Genetics, and especially the contributions of Katie DeKruyff, for their support with designing and conducting the pig experiments.

Author contributions

B.R.S. and N.J.L. conceived the study. S.B., Y.Z., M.K., B.R.S., and N.J.L. designed and performed most of the experiments and helped write the manuscript. S.W. and F.A. performed the ^{18}F-FDG PET/CT imaging. L.M. provided critical reagents and advice on pig experiments. Additionally, M.L., T.A., L.L., G.S.K., F.W., J.Y., M.P., R.M., S.P., S.S.A., Y.K., A.I., C.F.B., N.G.L., C.F., R.B.C., Z.M., and L.B. helped design and perform experiments. B.R.S. and N.J.L. contributed equally as co-corresponding and co-senior authors.

Competing interests

N.J. Leeper is a co-founder and director of Bitterroot Bio Incorporated, a cardiovascular company studying macrophage checkpoint inhibition. Stanford University (B.R. Smith, N.J. Leeper) has filed patents relating to the role of pro-efferocytic nanotherapies for cardiovascular disease. The remaining authors declare no competing interests.

Additional information

Supplementary information The online version contains supplementary material available at https://doi.org/10.1038/s41467-024-52005-1.

Correspondence and requests for materials should be addressed to Bryan Ronain Smith or Nicholas J. Leeper.

Peer review information *Nature Communications* thanks Jacob Bentzon and the other, anonymous, reviewer(s) for their contribution to the peer review of this work. A peer review file is available.

Reprints and permissions information is available at http://www.nature.com/reprints

Publisher's note Springer Nature remains neutral with regard to jurisdictional claims in published maps and institutional affiliations.

Open Access This article is licensed under a Creative Commons Attribution-NonCommercial-NoDerivatives 4.0 International License, which permits any non-commercial use, sharing, distribution and reproduction in any medium or format, as long as you give appropriate credit to the original author(s) and the source, provide a link to the Creative Commons licence, and indicate if you modified the licensed material. You do not have permission under this licence to share adapted material derived from this article or parts of it. The images or other third party material in this article are included in the article's Creative Commons licence, unless indicated otherwise in a credit line to the material. If material is not included in the article's Creative Commons licence and your intended use is not permitted by statutory regulation or exceeds the permitted use, you will need to obtain permission directly from the copyright holder. To view a copy of this licence, visit http://creativecommons.org/licenses/by-nc-nd/4.0/.

© The Author(s) 2024